Int. J. Solids Structures Vol. 30, No. 24, pp. 3475–3489, 1993
Printed in Great Britain

0020–7683/93 $6.00+ .00

STRAIN HARDENING IN THE MOVING HINGE METHOD

A. N. SHERBOURNE and F. LU†
Department of Civil Engineering, University of Waterloo, Waterloo, Ontario N2L 3G1, Canada

(*Received* 7 *December* 1992; *in revised form* 25 *June* 1993)

Abstract—The moving hinge method is very effective in dealing with large displacement problems. However, it appears that this method has been mainly applied for a rigid–perfectly plastic material, despite some earlier attempts to consider a strain hardening material. The purpose of this paper is to expound on the effect of strain hardening, and, to incorporate it into the moving hinge equation. In order to do so, the energy dissipation during the curvature jump at the moving hinge is treated as a loading/reverse loading process over an infinitesimal duration of load application. The proposed method accounts for both isotropically and kinematically hardening materials. Experiments on aluminum rings compressed between two wedges are performed to validate the adequacy of the analysis. The results indicate a favourable agreement between the analysis and experiments. It should be noted that the present analysis gives an upper bound solution. Caution should be exercised since the accuracy depends on the chosen deformation mode.

NOMENCLATURE

A, B, C	location points, defined in relevant figures
a_1, a_2	constants introduced in eqn (22)
A_H	work done in a moving hinge, see Figs 2(b, c)
A_s	work done in an arc, see Fig. 2(a)
b, h	width and depth of a rectangular section
b_1, b_2, b_3	constants introduced in eqn (34)
E	Young's modulus
E_H	energy dissipated in a moving hinge
E_p	plastic modulus
E_pI	hardening flexural rigidity
E_S	energy dissipated in an arc
H	moving hinge
I	$= bh^3/12$
K	curvature
K^+, K^-	curvature before and after the jump at the hinge
M	bending moment
M_i, M_j, M_k	moments illustrated in Fig. 3
M_p	full plastic moment, $= bh^2\sigma_y/4$
P	applied load
P_o	initial collapse load, $= 4M_p/R_o$
R_o	initial radius
R_1, R_2, R_3	radii defined in Fig. 6
S	arc length, or natural coordinate
S_1, S_2, S_3	arc lengths defined in Fig. 6
t	time
W	energy
X, Y	coordinates defined in Fig. 12
α	hardening factor, $= E_pI/M_pR_o$
Δ	deflection
ε, σ	strain and stress
θ_o	constant introduced in eqn (22)
$\theta_1, \theta_2, \theta_3$	arc span angles defined in Fig. 6
σ_y	yield stress

INTRODUCTION

In problems of plastic deformation, it is traditionally assumed that the material is rigid (or elastic)–perfectly plastic. Strain hardening behaviour is not usually considered because of its greater complexity, or, because it is relatively unimportant in most situations. Furthermore, practitioners and designers are usually more interested in incipient collapse rather than the

† Current address: Department of Metals and Materials Engineering, University of British Columbia, Vancouver, B.C. V6T 1Z4, Canada.

extensive deformation which is associated with the loss of structural integrity. The neglect of strain hardening has spawned the maturing theory of limit analysis and design (Sobotka, 1989; Hodge, 1959).

However, when structural components are intended for use, for example, in impact situations as energy absorbers, the effect of strain hardening becomes significantly more important. This is not only because of the high strain rate involved, but because of the necessity to consider large displacement accompanying the impact action. The practical need to take strain hardening into account propelled more assiduous studies in this respect. For example, Reid and Reddy (1978) proposed a plastica theory in analysing the problem of a tube crushed between two rigid platens. This method, adapted from the elastica theory by analogy, can adequately include the strain hardening material parameter in analysis, thus improving the prediction of the load–displacement behaviour. Murray (1991) made an equivalently noteworthy contribution towards understanding the hardening effect in the problem of the column buckling into the large deflection range. More recently, a series of papers on the strain hardening effect were published (Sherbourne and Lu, 1993a, b; Lu and Sherbourne, 1992b, 1993), including the one on the reserve strength of dented tubular members which is a major concern in offshore engineering.

In view of the versatility of shape modelling, a more effective approach in dealing with large displacement problems is the moving hinge method. The idea of this method seems to have first appeared in a note by Abramowicz and Sawczuk (1981), and, it was later diligently advocated by Wierzbicki and Bhat (1986a, b) and Wierzbicki and Suh (1988). The fundamental aspects of its concept and usage have been discussed elsewhere (Lu and Sherbourne, 1992a). This method is essentially an upper bound approach by assuming a kinematically admissible deformation mode. The so-called moving hinge is a curvature discontinuity that connects two adjacent segments of uniform curvature and travels along a structural element such as an arch. The moving hinge method was introduced, and has been mainly applied, for a rigid-perfectly plastic material. In order to accommodate strain hardening in some situations where hardening is an important factor in predicting structural behaviour, the moving hinge equation, which involves the hinge travelling speed and the difference between adjacent curvatures, has to be modified. Although some efforts were made by Wierzbicki and Bhat (1986a) to consider, in an approximate manner, the strain hardening effect, the true nature of the moving hinge behaviour was not explained. The argument in their analysis appears to be flimsy since a unique bending moment has been assigned to a moving hinge. In reality, there exists a moment jump or moment discontinuity at the hinge.

In this paper, a method is proposed to incorporate the strain hardening effect. The curvature jump phenomenon at the moving hinge is explained in terms of a loading/reverse loading process so that the moving hinge equation for the perfectly plastic material can be extended to include the hardening property. Both isotropic and kinematic hardening are discussed.

BASIC EQUATIONS

If a solid body is subjected to a concentrated load, P, the equilibrium state can be established by applying the energy balance principle

$$W_{\text{int}} + W_{\text{ext}} = 0 \tag{1}$$

where W_{int} and W_{ext} are the internal and external work, respectively.

If the stress and strain in the differential volume, $\mathrm{d}V$, are expressed as σ and ε, and the deflection in the direction of the load as Δ, we have:

$$W_{\text{int}} = -\int_V \int_0^t \sigma \dot{\varepsilon}\, \mathrm{d}t\, \mathrm{d}V, \tag{2}$$

and

$$W_{\text{ext}} = \int_0^t P\dot{\Delta}\,\mathrm{d}t, \tag{3}$$

where the upper dot signifies the time derivative, $\mathrm{d}/\mathrm{d}t$.

Substitution of eqns (2) and (3) into eqn (1) leads to:

$$\int_0^t P\dot{\Delta}\,\mathrm{d}t = \int_V \int_0^t \sigma\dot{\varepsilon}\,\mathrm{d}t\,\mathrm{d}V. \tag{4}$$

For a structural member, such as the arch shown in Fig. 1, the stress (σ) and strain (ε) should be replaced with the bending moment (M) and its corresponding curvature (K). Equation (4) thus becomes:

$$\int_0^t P\dot{\Delta}\,\mathrm{d}t = \int_S \int_0^t M\dot{K}\,\mathrm{d}t\,\mathrm{d}S, \tag{5}$$

where S is the arc length.

For a continuous system, mere differentiation with respect to time on both sides of eqn (5) leads to:

$$P = \frac{1}{\dot{\Delta}} \int_S M\dot{K}\,\mathrm{d}S. \tag{6}$$

If, however, the system is discontinuous at certain points, such as the moving hinge locations, differentiation has to be done piecewise for the continuous segments of arc and separately for the movement of the discontinuities. Consider again the flexible arch, AB, of rectangular section b(width) $\times$ h(depth), under a single load, P, at the tip (Fig. 1). Suppose that it contains a moving hinge, H, travelling in the direction as shown in the figure with adjacent curvatures K^- and K^+. It was derived in an earlier study (Lu and Sherbourne, 1992a) that, for a rigid–perfectly plastic material,

$$P\dot{\Delta} = M_p \int_A^B |\dot{K}|\,\mathrm{d}S + M_p\dot{H}|K^- - K^+|, \tag{7}$$

where $M_p = bh^2\sigma_y/4$ and $\dot{H}$ with the upper dot represents the travelling speed of the hinge. The two terms on the right side of eqn (7) stand for, respectively, the energy (E_S) dissipated in the continuous change in the arc, AB, and the energy (E_H) consumed in the travelling hinge, H. Absolute values have to be used for each term to signify the positivity of the plastic energy loss.

For a strain hardening material, difficulties arise from the coupling between the bending moment and curvature. Since the whole deformation history, rather than just the deformation rate, has to be considered, the original curvature, K_o, also plays a role. In order to

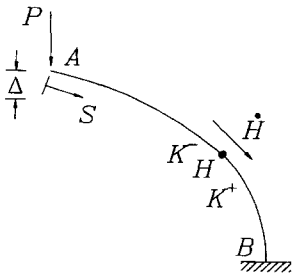

Fig. 1. Flexible arch under a single load.

resolve this problem, let us investigate how plastic energy is dissipated in the continuous segments and at the moving hinges.

The rate of energy dissipation in eqn (7) can be alternatively expressed in incremental form over an infinitesimal time interval, dt,

$$dE_S = \dot{E}_S dt = \int_A^B M_p |\dot{K}| \, dt \, dS = \int_A^B dA_S \, dS, \tag{8}$$

$$dE_H = \dot{E}_H dt = M_p |K^- - K^+| \, \dot{H} \, dt = A_H \, dS, \tag{9}$$

where

$$dA_S = \dot{A}_S dt = M_p |\dot{K}| \, dt, \tag{10}$$

$$A_H = M_p |K^- - K^+|, \tag{11}$$

and

$$dS = \dot{S} dt = \dot{H} dt. \tag{12}$$

It can be seen that dA_S and A_H are the shaded areas indicated in the moment–curvature relations shown in Fig. 2. Figure 2(a) shows the change of curvature, K, at any point in AB from the original, K_o to the current K_S, except for the point H. Because of the rigid–perfectly plastic assumption, the moment at any point in AB is M_p. The increment of plastic work done in the instant dt over a differential arc length dS is ($dA_S \, dS$), as given by eqn (8). The situation at point H, however, is quite different, depending on whether there is a positive or negative curvature jump, as shown in Figs 2(b, c) for the curvature history at point H. Suppose the hinge moves in the direction shown in Fig. 1, the curvature reaches K^+ first before it jumps instantaneously from K^+ to K^-. Such a jump can be seen as simply a loading [Fig. 2(b)] or reverse loading [Fig. 2(c)] process depending on the relative magnitude of the curvature before (K^+) and after (K^-) the jump. The resulting plastic work dissipated in the jump process is ($A_H \, dS$), as expressed by eqns (9), (11) and (12).

This knowledge can be extended analogously to a rigid–strain hardening material with the flexural hardening rigidity, E_pI. For the deformation in the continuous segments, eqn (10) should be revised as [see Fig. 3(a)]

$$dA_S = |M\dot{K}| \, dt. \tag{13}$$

The moment, M, is as follows due to hardening:

$$M = M_p[1 + \alpha R_o(K_S - K_o)], \tag{14}$$

where $\alpha = E_pI/(M_pR_o) = E_ph/(3\sigma_yR_o)$ is a hardening factor.

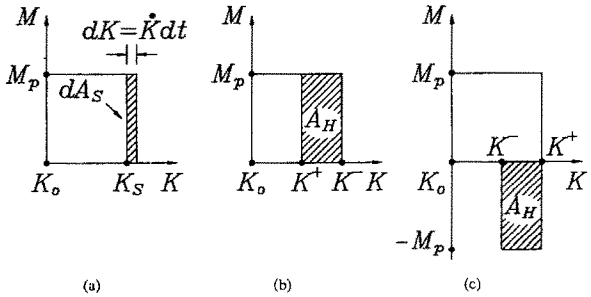

Fig. 2. M vs K for a rigid perfectly plastic material.

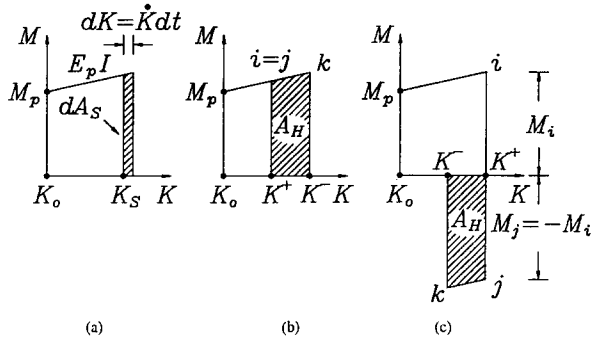

Fig. 3. M vs K for an isotropic hardening material.

Equations (13) and (14) can be used for both types of hardening, isotropic and kinematic. For the moving hinges, however, these two hardenings have to be considered separately because of their distinct characteristics of reverse loading.

For isotropic hardening, the moment–curvature relations are shown in Figs 3(b, c), where the curvature jump process is completed from point i to point k. In the loading process where points i and j coincide, $M_j = M_i$. In the case of reverse loading, isotropic hardening requires that, $M_j = -M_i$. In either case, we have:

$$M_k = M_j + E_p I(K^- - K^+). \tag{15}$$

The corresponding shaded areas are sketched in Figs 3(b, c), respectively for the above two cases and can be obtained as follows:

$$A_H = \tfrac{1}{2}|M_j + M_k||K^- - K^+| = |M_j + \tfrac{1}{2}E_p I(K^- - K^+)|\,|K^- - K^+|. \tag{16}$$

For kinematic hardening, the expressions need some modifications. The loading process is the same as for isotropic hardening, i.e. $M_j = M_i$. In the unloading process, the current moment will drop twice the fully plastic value. Thus, $M_j = M_i - 2M_p$. For the situations shown in Figs 4(a, c) where M_j and M_k have the same signs, we have the identical expression as eqn (16), i.e.

$$A_H = \tfrac{1}{2}|M_j + M_k|\,|K^- - K^+| = |M_j + \tfrac{1}{2}E_p I(K^- - K^+)|\,|K^- - K^+|. \tag{17}$$

In the case where M_j and M_k have the opposite signs [Fig. 4(b)], we have instead:

$$A_H = \left|\frac{M_j M_k}{E_p I} + \tfrac{1}{2}E_p I(K^- - K^+)^2\right|. \tag{18}$$

Equations (14)–(18) will take the same form if the initial and subsequent moment is negative, except that M_p should be replaced by $-M_p$.

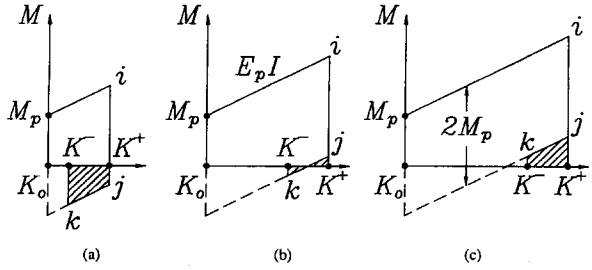

Fig. 4. M vs K for a kinematic hardening material.

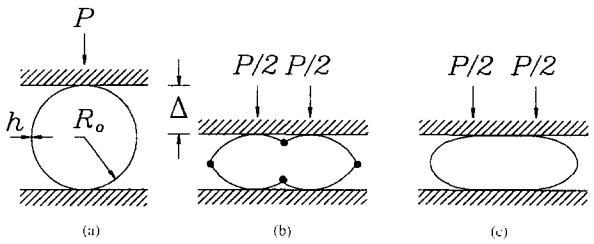

Fig. 5. Deformation mode of a crushed ring.

RING CRUSHED BETWEEN TWO RIGID PLATES

To demonstrate the use of the moving hinge method with strain hardening taken into account, consider the problem of a ring crushed between two rigid plates [Fig. 5(a)], which has been tackled by a number of researchers with different approaches. Although such a problem had been attempted numerically at an earlier time (Mutchler, 1960), a full theoretical investigation was initiated by DeRuntz and Hodge (1963), who used a limit analysis approach. Their suggested four-hinge mechanism [Fig. 5(b)], which takes into account the geometrical stiffening effect, gave rise to the foundation-laying yet underestimating load–displacement curve as compared with experimental values. Redwood (1964) confirmed the experimental data by referring to the experiments performed by Burton and Craig (Redwood 1964) but questioned the four-hinge model. Efforts were thus made to correct this discrepancy by considering, rather empirically, an alternative deformation mechanism [Fig. 5(c)] in which strain hardening can be taken into account. Despite the seemingly right choice of the plastic hinge length, the curve still fell short of experiment. This problem was later re-examined extensively by Reid and Reddy (1978) who proposed the ring crushing plastica theory. By applying the idea of the standard elastica theory, expounded by Frisch-Fay (1962), to the deformation mode in Fig. 5(c), one is able to replace the side plastic hinges with plastic regions that are strain hardening. The deformation of the strain hardening segment is assumed to consist of two parts: perfectly plastic and strain hardening deformations. Thus, the strain hardening deformation can be analyzed in the same way as in elastica, with EI replaced by E_pI. In all these approaches, the methodology remains the same i.e. a deformation mode is assumed and then the applied force is calculated considering the equilibrium of the mechanism. While this so-called inverse method is commonly accepted in dealing with large deformation problems, a valid question here is whether the assumed shape is a realistic one. The ring tests of the present authors and others all confirmed that the actual deformation fits neither the four-hinge mechanism nor the pattern proposed in the plastica theory. Instead, a "peanut" or "dumbbell" shape of the deformed ring is usually observed in experiments. In this regard, the moving hinge method is preferred because of its capacity for modelling various deformation modes.

MOVING HINGE DEFORMATION MODEL

A typical deformed shape of the ring is shown in Fig. 6 where only a quarter ring will be considered in the calculation owing to double symmetry. Because of the distinct curvature

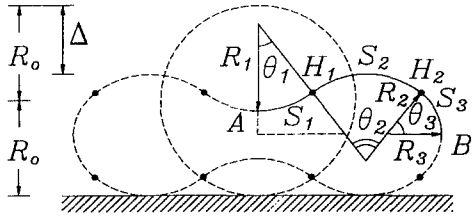

Fig. 6. Moving hinge modelling.

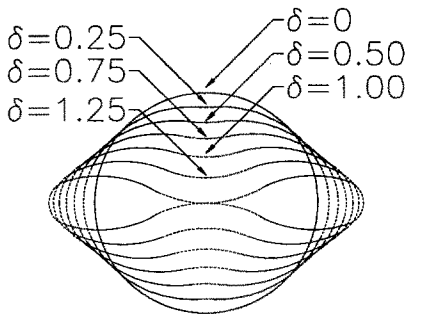

Fig. 7. Progressive shape change from moving hinge modelling.

characteristics for the three segments, AH_1, H_1H_2 and H_2B, it is necessary to have at least two moving hinges, H_1 and H_2, for the quarter ring in order to adequately model the shape. Using the notations shown in the figure and assuming the convex part (H_1H_2 and H_2B) as having a positive curvature (or radius), the geometric compatibility requires that:

$$\theta_1 = \frac{1}{R_2 - R_1}\left[\frac{\pi}{2}(R_0 - R_2) + \theta_3(R_2 - R_3)\right], \tag{19}$$

$$\theta_2 = \frac{1}{R_2 - R_1}\left[\frac{\pi}{2}(R_o - R_1) + \theta_3(R_1 - R_3)\right] \tag{20}$$

where R_o is the initial radius of the ring; and R_i and θ_i ($i = 1, 2, 3$) are the radii and span angles for the arcs AH_1, H_1H_2 and H_2B, as illustrated in Fig. 6. The total deflection is:

$$\Delta = 2[R_o - R_2 + (R_2 - R_3)\sin\theta_3]. \tag{21}$$

Based on the proposed deformation pattern (Fig. 6) and the actual shape change observed experimentally, the following equations are chosen to represent the deformation:

$$R_1 = (-1 + a_1\theta_3)R_o, \quad R_2 = (1 + a_1\theta_3^2)R_o, \quad R_3 = \frac{\left(1 - \dfrac{2\theta_3}{\pi}\right)^{a_2}}{1 - \dfrac{2\theta_o}{\pi}} R_o, \tag{22}$$

where the constants a_1, a_2 and θ_o are adjustable parameters that should be selected according to the measurements from experiments. Using θ_3 as the control variable, the deformation pattern and progression can be completely determined. For example, if we let $a_1 = \theta_o = 0$ and $a_2 = 1$, the resulting deformation shapes are calculated at various stages. They are then plotted in Fig. 7 for $\Delta/R_o = 0$, 0.25, 0.50, 0.75, 1.00, 1.25 and 1.513 (ultimate). The intersection points of the alternating broken and solid curves represent moving hinge locations. Referring to the first quadrant in Fig. 6, the two moving hinges, H_1 and H_2, originate, respectively, at the material points A and B. Such a pattern is also revealed correspondingly by the gradual spreading of the broken-line segments in Fig. 7, as the deformation progresses. The ultimate deflection, $\Delta/R_o = 1.513$, signifies the touching of the top and bottom centre points. The condition for touching is:

$$R_o - \frac{\Delta}{2} - (R_1 + R_2)(1 - \cos\theta_1) = 0. \tag{23}$$

The total applied load can be expressed according to eqn (6) as follows:

$$P = \frac{4}{\dot{\Delta}}(|\dot{A}_{S_1}S_1| + |\dot{A}_{S_2}S_2| + |\dot{A}_{S_3}S_3| + |A_{H_1}\dot{S}_1| + |A_{H_2}\dot{S}_3|). \tag{24}$$

Evaluation of each term in eqn (24) should be based on eqns (7–18) for various material types. For a perfectly plastic material, in particular, an explicit solution can be obtained since the bending moment maintains a fully plastic value and can be factored out of each term in eqn (24). Thus:

$$P = \frac{4M_p}{\dot{\Delta}}(|\dot{K}_1S_1| + |\dot{K}_2S_2| + |\dot{K}_3S_3| + |(\dot{K}_1 - K_2)\dot{S}_1| + |(K_3 - K_2)\dot{S}_3|), \tag{25}$$

where

$$K_1 = \frac{1}{R_1}, \quad K_2 = \frac{1}{R_2}, \quad K_3 = \frac{1}{R_3}, \tag{26}$$

are the curvatures of the three arcs and

$$S_1 = -\theta_1 R_1, \quad S_2 = \theta_2 R_2, \quad S_3 = \theta_3 R_3. \tag{27}$$

Note that R_1 is itself negative.

In calculation, the rate of deformational quantities can be obtained by differentiating with respect to the time-like parameter, θ_3. For instance,

$$\dot{\theta}_1 = \frac{\dot{R}_1 - \dot{R}_2}{(R_2 - R_1)^2}\left[\frac{\pi}{2}(R_o - R_2) + \theta_3(R_2 - R_3)\right] + \frac{1}{R_2 - R_1}\left[R_2 - R_3 + \theta_3(\dot{R}_2 - \dot{R}_3) - \frac{\pi}{2}\dot{R}_2\right], \tag{28}$$

$$\dot{\theta}_2 = \frac{\dot{R}_1 - \dot{R}_2}{(R_2 - R_1)^2}\left[\frac{\pi}{2}(R_o - R_1) + \theta_3(R_1 - R_3)\right] + \frac{1}{R_2 - R_1}\left[R_1 - R_3 + \theta_3(\dot{R}_1 - \dot{R}_3) - \frac{\pi}{2}\dot{R}_1\right], \tag{29}$$

$$\dot{\Delta} = 2[-\dot{R}_2 + (\dot{R}_2 - \dot{R}_3)\sin\theta_3 + (R_2 - R_3)\cos\theta_3]. \tag{30}$$

Incorporation of the deformation mode, as represented by eqn (22), into eqns (24) and (25) yields the applied load. A set of load–deflection curves are plotted in Fig. 8 for values of the hardening factor, α, at 0, 0.1 and 0.2. Note that the initial collapse load, $P_o = 4M_p/R_o$, from limit analysis and the initial radius, R_o, has been used to normalize the load–deflection curves. Apparently, isotropic hardening exhibits a more pronounced effect on the load–

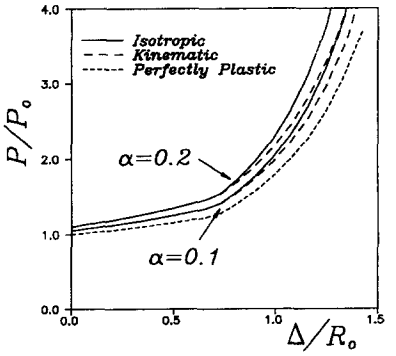

Fig. 8. Load vs deflection at various hardening levels.

deflection curve than kinematic hardening especially when Δ/R_o is higher than approximately 0.7. In the later stage, the arc S_3 starts to shrink, leading to unloading at hinge H_2. As can be seen from Figs 3 and 4, isotropic and kinematic hardening are differentiated only when unloading occurs. In reality, the load–deflection curve will probably lie somewhere between the isotropic and kinematic lines because of the ever-present Bauschinger effect.

EXPERIMENTS

The purpose of the experiment is two fold. First, it provides the necessary input data for analysis. The essential data needed in the present analysis are the deformation shapes and the material properties such as the yield stress and hardening modulus. The second purpose is to compare the analytical load–displacement results with the experimental data so that the presented approach can be verified. The experiment consists of two parts: ring tests and tensile tests.

Seamless aluminium alloy tubes (6061-T6) with 63.5 mm (2.5 in.) outside diameter and 1.65 mm (0.065 in.) thickness were used, of which 12.7 mm (0.5 in.) length rings were cut out as test specimens. The test set up consisted of two opposing wedges, a displacement transducer and a load cell. A hydraulic loading system with a hand pump was used. Because of the short ring length, the effect of two wedges are assumed to be the same as that of two rigid plates. Such an arrangement facilitated recording of the deformation shape during the test. Several interruptions are made during the ring test to allow the deformed shape to be imprinted onto graph paper by india ink. The computer-reproduced record of one representative deformation history is shown in Fig. 9.

The necessary material properties are obtained from simple tension tests. Four longitudinal tension specimens were directly cut out of the tubes from the same batch as those for the ring tests. The specimens were prepared and tested according to ASTM standard B577. The yield strength is conventionally taken at an off-set of 0.2% strain, as illustrated in Fig. 10(a) for a typical stress–strain curve. Since a rigid–linear strain hardening material model is used, it is appropriate to derive the yield stress and hardening (or plastic) modulus according to Fig. 10(b), where the hardening line is extended to intersect the ordinate. The resulting average values for the yield stress, σ_y, and the plastic modulus, E_p, are 290 MPa

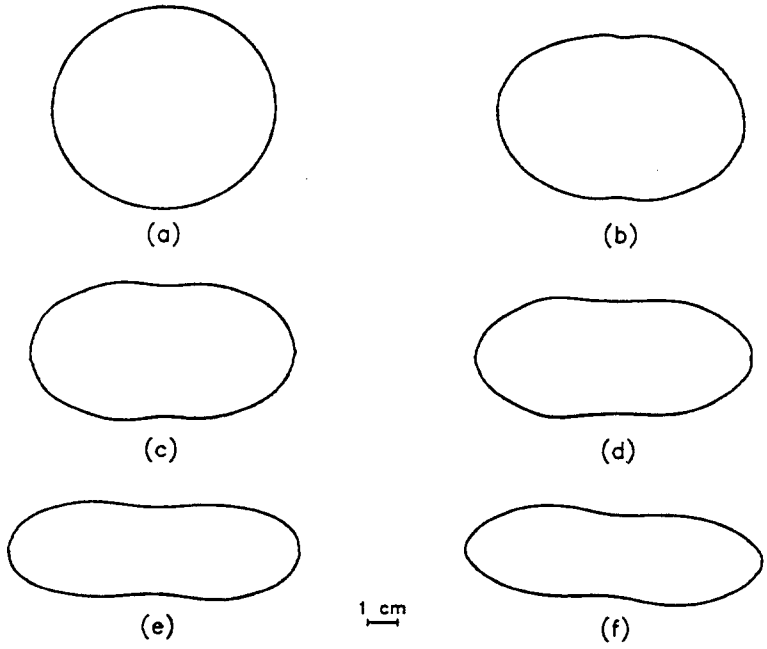

Fig. 9. Representative shape change from experiments.

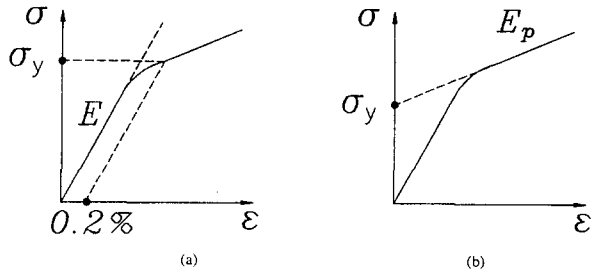

Fig. 10. Typical stress–strain relationship from tensile tests.

and 500 MPa, respectively. The elastic modulus, E, is ignored. The fully plastic moment and the initial collapse load can now be evaluated, respectively, as follows:

$$M_p = \tfrac{1}{4}\sigma_y bh^2 = \frac{290 \times 12.7 \times 1.651^2}{4} = 2510\,(\text{kN}\cdot\text{mm}) \tag{31}$$

and

$$P_o = \frac{4M_p}{R_o} = \frac{4 \times 2510}{31.75} = 316\,(\text{kN}). \tag{32}$$

COMPARISONS WITH OTHER THEORIES

It can be seen, by comparing Figs 7 and 9, that the assumed deformation mode and the experimentally measured ring shapes are in reasonable agreement. Therefore, the same procedure can be used to obtain the load–deflection curves for aforementioned three types of material modelling. Modification is made to the hardening factor, α. We have:

$$\alpha = \frac{1}{3}\frac{E_p h}{\sigma_y R_o} = \frac{500 \times 1.651}{3 \times 290 \times 31.75} = 0.03. \tag{33}$$

The results are presented in Fig. 11 together with the experimental data from the three ring tests described before. The agreement seems to be good for the most part (note that the elastic effect is ignored). Therefore, the moving hinge prediction curves will be used later for comparisons with other theories.

The extent of the strain hardening effect depends on the values of the plastic modulus to yield stress ratio, E_p/σ_y, and the thickness to radius ratio, h/R_o. The value of 1.76 for E_p/σ_y (T6-6061 aluminum) is very low in comparison with steels. The mild steel specimens used by Reid and Reddy (1978) were reported to have a much higher hardening effect ($E_p/\sigma_y = 6.15$). Therefore, the present strain hardening analysis may be more useful for steel

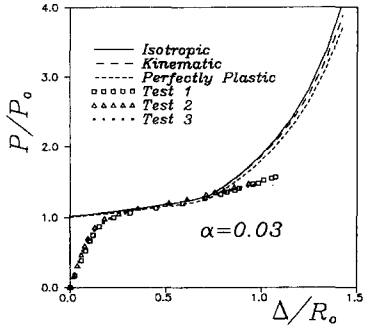

Fig. 11. Comparison with experiments.

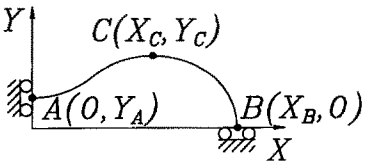

Fig. 12. Coordinates for continuous analysis.

rings or short tubes. A greater thickness to radius ratio would also warrant consideration of strain hardening.

It is observed that, at $\Delta/R_o \approx 0.7$, there appears to be a kink in the moving hinge solution (e.g. the solid line in Fig. 13). This is because, from this point on, S_3 starts to decrease and the corresponding curvature rate accelerates more rapidly. This rapid strengthening behaviour at the later stage of deformation is readily observable in a ring made of more ductile material (Lu, 1993). In the present case, when the deformation becomes excessive, the two side regions (near point B in Fig. 6) were observed to develop crazes (fine surface cracks), which is probably the reason for the discrepancy in the later stage of deformation.

Continuous analysis (Sherbourne, Lu and Dubey, 1991)

Another way of calculating the load is to directly integrate eqn (6), which requires a numerical scheme. The curvature history can be obtained by choosing a particular curve form controlled by a few parameters that change with the progression of the deformation. It is found that the consistent "peanut" pattern of the deformation shape can be represented with the kinematically admissible Cassinian curve, described by the following equation

$$[(b_1X-b_2)^2+Y^2][(b_1X+b_2)^2+Y^2] = b_3^4 \tag{34}$$

where b_1, b_2 and b_3 are constants subject to change for any particular deformation stage. The form of such a curve automatically satisfies the nonrotation conditions at the boundary points A and B (Fig. 12), i.e. $\mathrm{d}Y/\mathrm{d}X = 0$ at $X = 0$ and $\mathrm{d}X/\mathrm{d}Y = 0$ at $Y = 0$. To fit the Cassinian curve to a measured shape, values of b_1, b_2 and b_3 are selected so that the coordinate values at points A, B and C (Fig. 12) match with the measured ones. This process involves trial and error since the axial inextensibility of the ring has to be simultaneously satisfied and checked for each fit. This condition requires that:

$$\int_A^B \sqrt{1+(\dot{Y}')^2}\,\mathrm{d}X = \frac{\pi}{2}R_o. \tag{35}$$

It should be noted that, of the four coordinate values, Y_A, X_B, X_C and Y_C, only three can be fitted to the experimental measurements since there are only three control parameters in eqn (34). Table 1 compares the values of Y_A, X_B and Y_C for the modelling and the experiments. The experimental measurements have been averaged based on the three tests conducted.

Table 1. Modelling of the deformed shape

	Modelled			Measured		
Δ/R_o	Y_A/R_o	Y_C/R_o	X_B/R_o	Y_A/R_o	Y_C/R_o	X_B/R_o
0.46	0.77	0.77	1.13	0.76	0.77	1.19
0.72	0.62	0.64	1.22	0.60	0.62	1.25
0.90	0.51	0.55	1.28	0.50	0.54	1.34
1.00	0.44	0.50	1.31	0.43	0.49	1.37
1.10	0.39	0.45	1.35	0.36	0.43	1.39

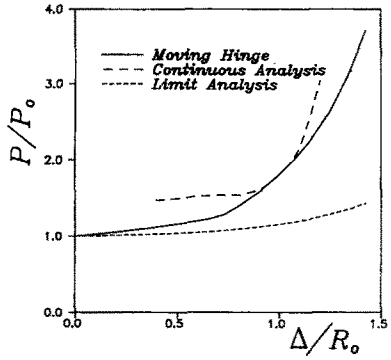

Fig. 13. Rigid–perfectly plastic analysis.

The load–deflection curve from the continuous analysis, shown in Fig. 13, is obtained according to the rigid–perfectly plastic assumption. The effect of strain hardening is not considered because, to take strain hardening into account, requires more complete and sensitive shape measurements in the experiments. Unlike the perfect plastic analysis which requires only the rate of the deformational quantities, the entire deformation history is now necessary. The need of a sensitive measuring system is apparent from the lack of agreement between the results of the continuous analysis and those of the moving hinge method. Only a segment of the curve is in perfect touch with the curve from the moving hinge method.

In another related tube crushing problem, a numerical procedure is proposed by Lu (1993) to consider the elastic and strain hardening effects. In this case, the cross-sectional shape is assumed to be elliptical Therefore, the computation is mathematically more tractable.

Limit analysis (DeRuntz and Hodge, 1963)

The limit analysis solution provided by DeRuntz and Hodge (1963) reveals conveniently the qualitative behaviour of a crushed ring by the following expression:

$$P = \frac{4M_p}{R_o}\left[1-\left(\frac{\Delta}{2R_o}\right)^2\right]^{-1/2}. \tag{36}$$

However, the load–deflection curve generated using eqn (36) lies well below the moving hinge curve. This is caused by over-idealization of the ring shape. An actual deformation is usually continuous and a true plastic hinge can never form. The four hinge mechanism requires less load to advance the displacement.

Plastica theory (Reid and Reddy, 1978)

By using the following moment–curvature relation in the hardening range ($M \geqslant M_p$):

$$K = \frac{M - M_p}{E_p I}, \tag{37}$$

and the method of elastica, Reid and Reddy (1978) derived a set of self-contained equations to calculate the deflection from a specified load. These equations are easy to use and therefore the load–deflection curve is reproduced here incorporating the current material properties. The key parameter, mR_o, as used by Reid and Reddy as a material/geometry indicator, is:

$$mR_o = \sqrt{\frac{6\sigma_y R_o}{E_p h}} = \sqrt{\frac{6\times 290\times 31.75}{500\times 1.651}} = 8.2. \tag{38}$$

The nondimensional load value, P/P_o, is first selected from 1.0 and up. Some inter-

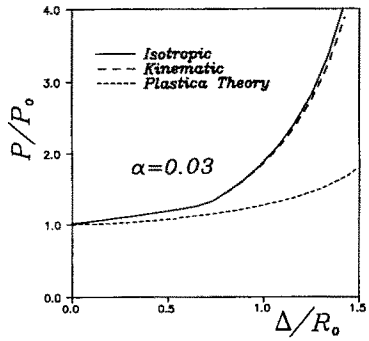

Fig. 14. Comparison with the plastica theory.

mediate values are calculated. In the process, the elliptical integrals of the first and second kind are obtained from the handbook by Belyakov (1965). The eventual result is the nondimensional deflection, Δ/R_o. The generated curve is plotted in Fig. 14. Although this curve underestimates the load, the one produced by Reid and Reddy was very close to their experimental data. In their calculation, mR_o was taken as 3.30 which indicates a higher strain hardening effect. This illustrates the importance of considering strain hardening for mild steels.

VALIDITY AND ACCURACY OF THE STRAIN HARDENING FORMULATION

As has been mentioned in the introduction, a moving hinge is a curvature discontinuity or jump. It is not a plastic hinge in a conventional sense. The presence of the curvature discontinuity lead to a corresponding discontinuity of the bending moment at the hinge. Depending on the nature of the curvature jump, the moment discontinuity may appear in different forms. If there is a drop of curvature in the jump process, the subsequent moment will have an opposite sign [Figs 2(c) and 3(c)]. However, if there is a decrease of curvature, the plastic moment maintains the same sign [Figs 2(b) and 3(b)]. This feature shows the fundamental difference from the conventional plastic hinge at which the bending moments are always identical on the neighbouring sides.

In the paper by Lu and Sherbourne (1992a), the equations necessary to apply the moving hinge concept to a rigid–perfectly material are derived by both algebraic and graphic approaches. The change of sign for the bending moment at the moving hinge is unfortunately masked by the absolute symbol "| |". For a rigid–strain hardening material, the same procedure of proof becomes very cumbersome due to the variation of the bending moment. Besides, it will do little to disclose the actual deformation process at the hinge. Thus, the present energy approach has been proposed.

It should be pointed out that, in the present analysis, the continuous (arc) and discontinuous (moving hinge) parts have been considered separately. This procedure disregards the altered hardening behaviour in the continuous part due to the "load memory" left behind by the moving hinge. It can be illustrated by comparing the load histories of a quarter ring shown in Figs 15(a, b), where the lengths of the three arcs, S_1, S_2 and S_3, have been assumed to vary in the following way:

S_1 increasing from an initial zero length, $S_1(t_o) = 0$;
S_2 decreasing from a finite initial length;
S_3 decreasing from a finite initial length.

All the three corresponding curvatures, K_1, K_2 and K_3, increase as the deformation proceeds, with K_1 in the opposite direction of K_2 and K_3. The travelling direction of the two moving hinge hinges can be identified by examining the variations of the arc lengths.

Figure 15(a) demonstrates the actual moment change in each arc when the time t increases from t_o to t_3. The curved segments, e.g. *ab* and *ef* at $t = t_2$, of the M–S relationship are a result of continuously inheriting the moment existing before the jump. For example,

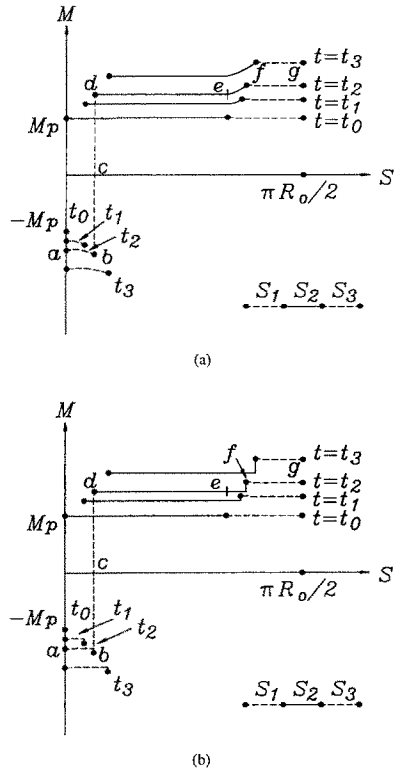

Fig. 15. Loading history in terms of M vs S relationship.

after a moment jumps from d, on the leading S_2, to b, on the trailing S_1, the moment at b will increase at the same rate as the entire segment ab. Since the curvature rate, or, moment rate, of S_2 is different from that in S_1, the range of ab will continue to grow from the end b. Note that the magnitude of cb is slightly higher than that of cd due to the instant hardening right after the jump at the hinge. The segment ef can be explained in a similar manner. In this case, f is not separated since S_2 and S_3 have the rates in the same direction.

Figure 15(b) reveals the adopted load history in the computational model where the curved parts have been replaced by the straight lines representing an uniformly distributed moment in a single arc.

Since the curvature is always uniform over a particular arc, S_i, the difference between these two cases [Figs 15(a, b)] is in effect reflected in the difference in the area encircled by the respective M–S curves. As can be seen, this discrepancy is expected to be very small, especially because the moment increases due to hardening is small compared to M_p. The diagrams in Fig. 15 have been exaggerated for the purpose of illustration.

In addition, this discrepancy only affects the part of the continuous change in the three arcs. The energy consumed in the curvature jump is accurately computed. It has been estimated that there is approximately an equal amount of energy dissipation in the continuous curvature change of the arcs and in the curvature jump, further reducing the scale of inaccuracy.

CONCLUSIONS

The influence of strain hardening may be significant depending on the combination of material, geometry and loading types. To incorporate such effects into the moving hinge method, the curvature jump at the hinge is approximated as a loading/reverse loading process. The derived equations are applied in the problem of a circular ring crushed betwen two rigid platens. The load–deflection results are in good agreement with experimental data. Comparisons with other theories on the same problem demonstrate that the use of

the moving hinge method allows for more flexibility while the accuracy and simplicity of computation are still maintained.

It should be borne in mind that all the available methods contain a certain level of arbitrariness in the assumption of the deformation mode. Various simplifications are necessary in order to achieve a workable solution. The main advantage of the moving hinge technique is its adaptability to various types of deformation modes. The axial tube crushing problem examined by Wierzbicki and Bhat (1986b) is a good example for the range of possibilities that this technique provides. The present extension of the moving hinge method to account for hardening allows one to deal with situations where strain hardening is an important part of the deformation and/or the effect of the thickness to radius ratio must also be considered.

Acknowledgements—The financial support from the Natural Sciences and Engineering Research Council of Canada through grant No. A-1582 is gratefully acknowledged.

REFERENCES

Abramowicz, W. and Sawczuk, A. (1981). On plastic inversion of cylinders. *Res. Mech. Lett.* **1,** 525–530.

Belyakov, V. M. (1965). *Tables of Elliptical Integrals—Part I.* Macmillan, New York, 554–593.

DeRuntz, J. A., Jr and Hodge, P. G., Jr (1963). Crushing of a tube between rigid plates. *J. Appl. Mech.* **30,** 391–395.

Frisch-Fay, R. (1962). *Flexible Bars.* Butterworths, London.

Hodge, P. G. (1959). *Plastic Analysis of Structures.* McGraw-Hill, New York.

Lu, F. (1993). *Large Plastic Deformation of Metal Tubes Used in Energy Absorbing Systems.* Ph.D. dissertation, University of Waterloo, Canada.

Lu, F. and Sherbourne, A. N. (1992a). Moving hinge in large displacement problems. *J. Engng Mech.* **118,** 1840–1849.

Lu, F. and Sherbourne, A. N. (1992b). Shear-bending interaction for strain hardening beams. *Int. J. Mech. Sci.* **34,** 789–804.

Lu, F. and Sherbourne, A. N. (1993). Load carrying capacity of strain hardening beams under shear, bending and axial forces. *J. Engng Mech.* **119** (in press).

Murray, N. W. (1991). The buckling of a pin-ended column of rectangular cross-section and strain hardening mild steel into the large-deflection range. *Thin-Walled Structs* **13,** 85–114.

Mutchler, L. D. (1960). Energy absorption of aluminum tubing. *J. Appl. Mech.* **27,** 740–743.

Redwood, R. G. (1964). Crushing of a tube between rigid plates. *J. Appl. Mech.* **31,** 357–358.

Reid, S. R. and Reddy, T. Y. (1978). Effect of strain hardening on the lateral compression of tubes between rigid plates. *Int. J. Solids Structs* **14,** 213–225.

Sherbourne, A. N. and Lu, F. (1993a). Effect of axial restraints on the deflection of strain hardening beams. *Int. J. Mech. Sci.* **35,** 397–413.

Sherbourne, A. N. and Lu, F. (1993b). Reserve strength of dented tubular members. Presented in *Fifth Int. Symp. on Tubular Structures*, August 1993, University of Nottingham, U.K.

Sherbourne, A. N., Lu, F. and Dubey, R. N. (1991). Large plastic deformation of short tubes and rings. *Proc. Progress in Struct. Engng* (Edited by D. E. Grierson, A. Franchi and P. Riva), pp. 423–435. Kluwer Academic Publishers, Dordrecht, The Netherlands.

Sobotka, Z. (1989). *Theory of Plasticity and Limit Design of Plates.* Elsevier, New York.

Wierzbicki, T. and Bhat, S. U. (1986a). Initiation and propagation of buckles in pipelines. *Int. J. Solids Structs* **22,** 985–1005.

Wierzbicki, T. and Bhat, S. U. (1986b). A moving hinge solution for axisymmetric crushing of tubes. *Int. J. Mech. Sci.* **28,** 135–151.

Wierzbicki, T. and Suh, M. S. (1988). Indentation of tubes under combined loading. *Int. J. Mech. Sci.* **39,** 229–248.